Geomechanics and Engineering, *Vol. 15, No. 1 (2018) 669-676*
DOI: https://doi.org/10.12989/gae.2018.15.1.669

Numerical analysis of a complex slope instability: Pseudo-wedge failure

Nima Babanouri* and Vahab Sarfarazi

Department of Mining Engineering, Hamedan University of Technology, Hamedan, Iran

(Received August 21, 2016, Revised May 12, 2017, Accepted November 20, 2017)

Abstract. The "pseudo-wedge" failure is a name for a complex instability occurring at the Sarcheshmeh open-pit mine (Iran). The pseudo-wedge failure contains both the rock bridge failure and sliding along pre-existing discontinuities. In this paper, a cross section of the failure area was first modeled using a bonded-particle method. The results indicated development of tensile cracks at the slope toe which explains the freedom of pseudo-wedge blocks to slide. Then, a three-dimensional discrete element method was used to perform a block analysis of the instability. The technique of shear strength reduction was used to calculate the factor of safety. Finally, the influence of geometrical characteristics of the mine wall on the pseudo-wedge failure was investigated. The safety factor significantly increases as the dip and dip direction of the wall decrease, and reaches an acceptable value with a 10-degree decrease of them.

Keywords: pseudo-wedge failure; bonded-particle model; rock bridge failure; discrete element method; slope stability

1. Introduction

Reinforcement corrosion has been identified as the main In general, rock slope instabilities can be categorized as three modes of material failure, structural failure, and mixed material-structural failure. In a material failure, the slip surface entirely passes through rock materials or rock masses with a great number of closely spaced discontinuities, behaving as continua (Wyllie and Mah 2004). A structural failure of rock slopes is, instead, controlled by major discontinuities of the rock mass (Agliardi *et al.* 2013). A mixed material-structural instability of rock slopes is caused by a combination of rock bridge failure and sliding along non-persistent rock discontinuities (Eberhardt *et al.* 2004, Stead *et al.* 2006).

Numerical modeling techniques have been widely used to solve complex slope problems, which otherwise, could not have been possible using conventional methods. Numerical methods of analysis used for rock slope stability investigations can be divided into two general approaches: continuum modeling and discontinuum modeling. Continuum modeling is best suited for the analysis of slopes that are comprised of massive intact rocks, soil-like or heavily fractured rock masses (Agliardi *et al.* 2013, Babanouri and Dehghani 2017, Blake 1968, Gao *et al.* 2016, García López-Davalillo *et al.* 2014, Jiang *et al.* 2015, Kanungo *et al.* 2013, Latha and Garaga 2010, Lombardi *et al.* 2017, Pain *et al.* 2014, Shamekhi and Tannant 2015, Stacey 1970, Tiwari and Latha 2016, Zheng *et al.* 2007). This method cannot handle many intersecting joints. In continuum models, the displacement field will always be continuous. For large slope deformations, the assumption of a continuum may not be realistic. The location of the failure surface can only be judged by the concentration of shear strain in the model. No actual failure surface discontinuity is formed (Sjöberg 1999).

Discontinuum modeling techniques such as the discrete element method (DEM) treat the rock slope as an assemblage of rigid or deformable blocks, and explicitly model discontinuities present in the rock mass. A DEM analysis includes sliding and opening of rock discontinuities controlled by the normal and shear stiffness of joints. It allows the deformation and movement of blocks, hence, is able to model complex mechanisms (Babanouri *et al.* 2013, Corkum and Martin 2004, Cundall 1988, Cundall and Strack 1979, Eberhardt *et al.* 2004, Faramarzi *et al.* 2016, Hart *et al.* 1988, Itasca Consulting Group Inc. 1999a, Wang *et al.* 2017).

The bonded-particle method is one of the variations of the discrete element methodology (Potyondy and Cundall 2004). It allows the rock to be represented as a series of spherical particles that interact through frictional sliding contacts. Clusters of particles may be bonded together through specified bond strengths in order to simulate joint bounded blocks. High stresses induced in the rock slope breaks the bonds between the particles simulating the intact fracture of the rock (Bonilla-Sierra *et al.* 2015, Huang *et al.* 2015, Potyondy and Cundall, 2004, Sarfarazi *et al.* 2014, Scholtès and Donzé 2015, Shi *et al.* 2016).

The western area of the Sarcheshmeh open-pit mine includes various types of failures, one of which is called the "pseudo-wedge" failure (Karimi Nasab 2001). Although most parts of the pseudo-wedge failure are kinematically infeasible, they have started to slide. In fact, the Sarcheshmeh pseudo-wedge failure contains both the intact rock failure and the sliding along pre-existing discontinuities. The repetition of near-parallel faults in the area has made the pseudo-wedge failure a challenge in expanding the western sector of the Sarcheshmeh mine. In

*Corresponding author, Assistant Professor
E-mail: babanouri@hut.ac.ir

ISSN: 2005-307X (Print), 2092-6219 (Online)

this research, a stress analysis of the pseudo-wedge failure was first carried out using a bonded-particle model in two dimensions. Then, a three-dimensional discrete element method was used to perform a block analysis of the instability. Finally, the influence of geometrical characteristics of the mine wall on the stability of the pseudo-wedge failure was investigated.

Fig. 1 Western wall of Sarchseshmeh copper mine and its pseudo-wedge failure (Wedge blocks have previously slid on the fault plane and cannot be seen in the photograph)

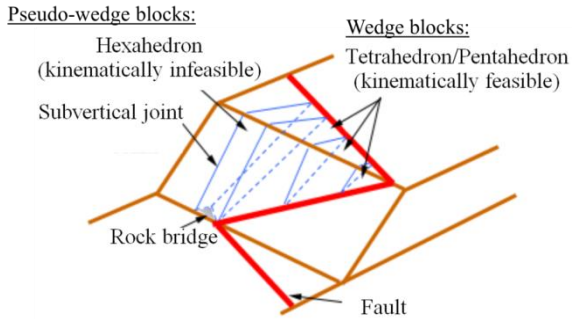

Fig. 2 Schematic illustration of Sarcheshmeh pseudo-wedge failure

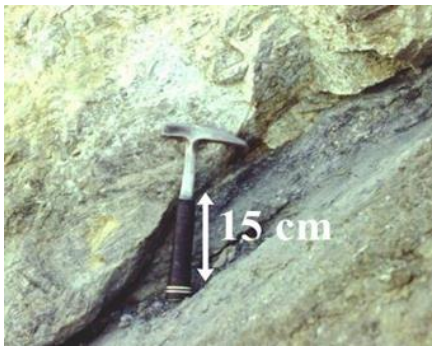

Fig. 3 Clay-infilled faults at Sarcheshmeh western area

Table 1 Dip and dip direction of fault, joint set, and slope face

Plane	Dip (°)	Dip direction (°)
Fault	45	75
Joint set	80	20
Slope face	65	40

2. Study area

The Sarcheshmeh copper deposit is the porphyry type, which is one of the most complex geological environments. The Sarcheshmeh deposit pertains to the late Tertiary granodioritic stock which intruded into the early Tertiary volcanics. The deposit was intruded by intra-mineralization and post mineralization dikes and intrusives (Shahabpour 1982). The original subcircular Sarcheshmeh porphyry stock exhibits an east-west elongation due to dilation by the dike swarm. The highest grade hypogene zone occurs as an annular ring in altered andesite around the periphery of the Sarcheshmeh stock (Waterman and Hamilton 1975).

As a result of intersection of a fault and a major joint set at the western wall of the Sarchseshmeh mine, several blocks have started to slide progressively (Fig. 1). This type of failure consists of large and loose blocks of weathered andesite. A wedge failure may occur along the line of intersection of two outward-dipping discontinuities that is cut by the slope face. However, the Sarcheshmeh pseudo-wedge failure continues to the areas where the intersection of the fault and joints has no daylight on the slope face, and are therefore kinematically infeasible (Fig. 2). In fact, a rock bridge exists at the base of pseudo-wedge blocks.

The bench height in the western wall of the Sarcheshmeh mine is 12.5 m. The fault is infilled by clayey material (with an average thickness of 15 cm) characterized by a friction angle (ϕ) of 20˚ and cohesion (c) of 14 kPa (Fig. 3). Dip and dip direction of the fault plane, joint set, and slope face are presented in Table 1.

3. Particle-bonded modeling

In order to investigate behavior of the rock bridge at the toe, a cross section of the infeasible areas of the failure was modeled in two-dimensional particle flow code (PFC2D). In this method, the rock is modeled as a set of bounded particles confined by external boundaries. The main bonding models implemented in PFC are contact-bond and parallel-bond. Contact bonds are used to represent the materials such as cement which attach particles on another. In contrast to parallel bonds, no radius or shear and normal stiffnesses are considered to contact bounds. A contact bond is characterized by its tensile and shear strength (Cundall and Strack 1999, Potyondy and Cundall 2004, Yoon 2007). The micro properties required for creating a contact-bonded particle model in PFC are: ball-to-ball contact modulus, stiffness ratio, ball friction coefficient, contact normal bond strength, contact shear bond strength, ratio of standard deviation to mean of bond strength both in normal and shear direction, and minimum ball radius (Potyondy and Cundall 2004). Three other micro parameters of parallel-bond radius multiplier, parallel bond modulus, and parallel-bond stiffness ratio need to be considered for generating a parallel-bonded particle model. The parallel-bond scheme was used to create bonded particle models in this study.

3.1 Generating particle-bonded model

Four stages are routinely followed to create a PFC2D

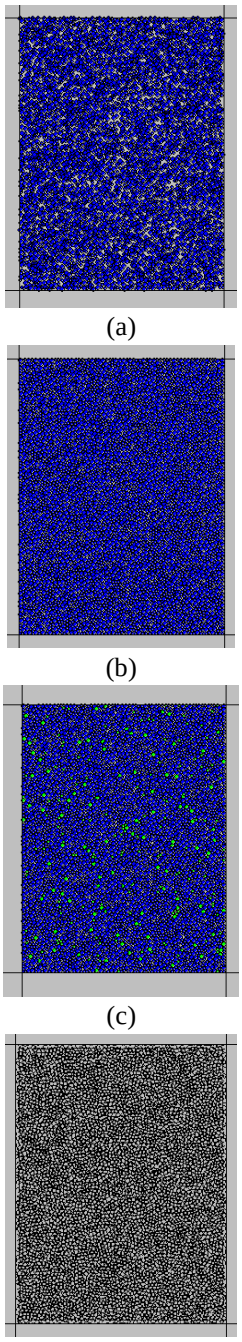

(a) (b) (c) (d)

Fig. 4 Stages of generating a PFC2D model of rock materials: (a) generating and packing the particles, (b) applying isotropic stress, (c) removal of floating particles and (d) forming bonds

model of rock materials, namely: (i) generating and packing the particles, (ii) applying isotropic stress, (iii) removal of floating particles, and (iv) forming bonds (Sarfarazi *et al.* 2014).

i) Generating and packing the particles (Fig. 4(a)): a rectangular box with frictionless sides was first created, and then filled by a series of particles. In order to avoid a large overlap between the particles and box boundaries, the boundary normal stiffness was set to be greater than the average particle normal stiffness. In order to ensure the appropriate packing of the particles, it is recommended that the ball positions and radii are drawn from uniform distributions throughout the model domain (Itasca Consulting Group Inc. 1999b). A uniform distribution was considered for particle diameters ranging between D_{min} and D_{max}. An overall porosity of 8% was assigned to the model in order to guarantee that the particles were sufficiently packed. It is worth mentioning that the assigned value of the model porosity does not necessarily represent the actual porosity of the rock material. The resulting porosity of the model after equilibration will not be identical to the specified porosity. This is due to the fact that balls will overlap in the equilibrated system (Itasca Consulting Group Inc. 1999b).

The particles were randomly distributed within the box at half their final diameter such that no two particles overlap. The particle sizes were then increased to their final values.

ii) Applying isotropic stress (Fig. 4(b)): to obtain a given value of isotropic stress, σ_0, defined as the average particle-to-particle stress, the whole particles were resized uniformly. The value of σ_0 is typically considered 1% of the uniaxial compressive strength of rock materials to be simulated. This is done to reduce the magnitude of the locked-in forces that will develop after the parallel bonds are added.

iii) Removal of floating particles (Fig. 4(c)): the model, at this stage, has many particles with one or two contacts which are considered as floating particles. To achieve a competent assembly of the particles, it is necessary to minimize the number of floating particles. By setting the number of ball contacts equal to 3 and the allowed number of floating particles to zero, a bonded assembly was obtain in which the balls away from the specimen boundaries had at least three contacts.

iv) Forming parallel bonds (Fig. 4(d)): parallel bonds were made between all adjacent particles.

Table 2 Micro properties used to represent rock material

Parameter	Value	Parameter	Value
Type of particle	Disc	Parallel-bond radius multiplier	1
Density (kg/m^3)	1,000	Young's modulus of parallel bond (GPa)	4
Minimum radius (mm)	0.27	Parallel bond stiffness ratio (pb_k_n/pb_k_s)	1.7
Size ratio	1.56	Particle friction coefficient	0.4
Porosity ratio	0.08	Parallel bond normal strength, mean (MPa)	5.6
Damping coefficient	0.7	Parallel bond normal strength, std. dev (MPa)	1.4
Contact Young's modulus (GPa)	4	Parallel bond shear strength, mean (MPa)	5.6
Stiffness ratio (k_n/k_s)	1.7	Parallel bond shear strength, std. dev (MPa)	1.4

3.2 Model calibration

Since the rock bridge at the toe was subjected to tensile stress, the model was calibrated using the Brazilian test. The actual Brazilian test was carried out on ten specimens according to the ISRM suggested method (ISRM 1978). By adjusting the micro properties listed in Table 2 according to the standard calibration procedures (Ghazvinian *et al.* 2012, Potyondy and Cundall 2004), a calibrated PFC particle

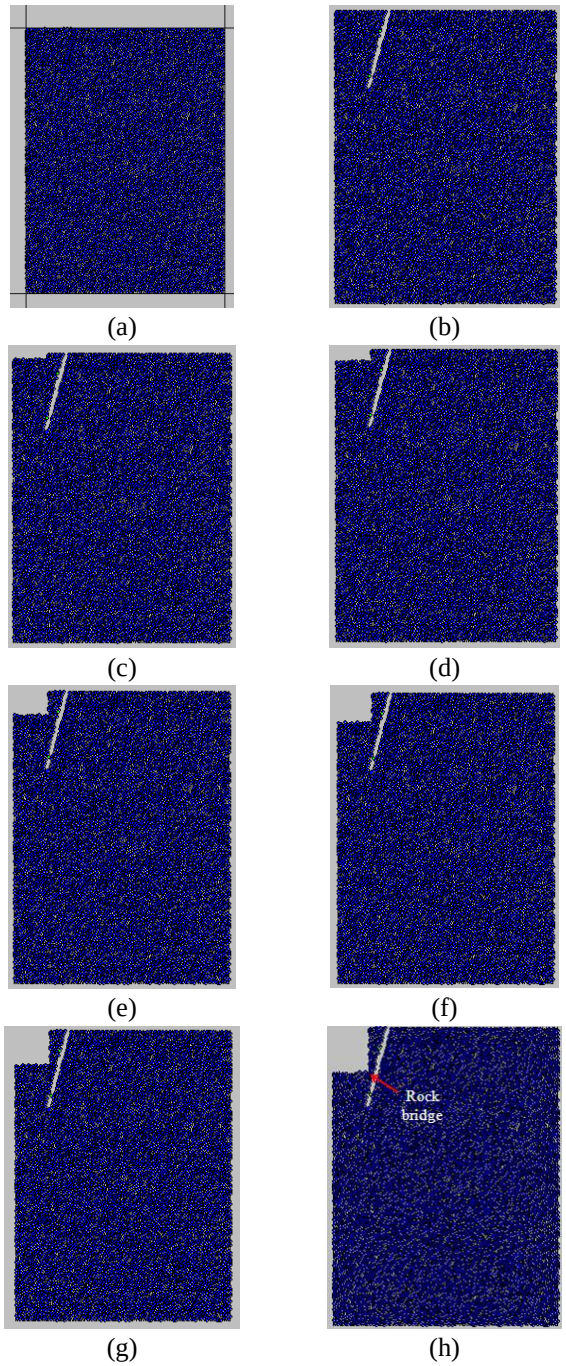

Fig. 5 Numerical simulation of rock slope with neighboring fault, (a) intact model, (b) fault generation and (c)-(h) sequence of rock slope excavation

assembly was obtained. The Brazilian disk had a diameter of 54 mm and consisted of 5,615 particles. Side boundaries of the model approached each other at a velocity of 0.016 m/s until the disk was split. The tensile strength of rock samples was nearly 1 MPa, and the tensile strength obtained from the numerical model was 1.1 MPa showing a good accordance between numerical and experimental results.

3.3 Simulation of rock slope with neighboring fault

After calibration of the model, a cross section of the rock slope with the neighboring fault was numerically simulated in PFC2D by creating a box of 75×100 m. A total of 11,179 disks with a minimum radius of 0.27 mm were used to construct the initial model (Fig. 5(a)). Then, the fault was entered the model with a length of 30 m (Fig. 5(b)). The rock slope was sequentially excavated in six stages (Fig. 5(c)-5(h)). In this way, the non-intrinsic forces were eliminated from the model. The fault has no daylight on the slope face, and a small rock bridge exists between the toe and the fault (Fig. 5(h)).

Fig. 6(a) shows the distribution of parallel bond force in the model at a state before the crack initiation. The black and red lines represent the compression and tensile forces, respectively. The bond force distribution in the model shows that a large tensile load was distributed in the rock bridge.

Fig. 6(b) shows progress of cracks in the model. Black lines represent the tensile cracks in the model. It is clear that under this condition, tensile cracks develop from the slope toe and coalesce into the fault. The cracks propagate nearly perpendicular to the fault plane. In fact, the gravitational effect of the rock slope and the torque around the rock bridges, bring the rock slope to failure. The formation of these new fractures at the toe explains the freedom of the pseudo-wedge blocks to slide. The results of further PFC analyses demonstrate that the failure will stop as the rock bridge width increases beyond 2.4 m.

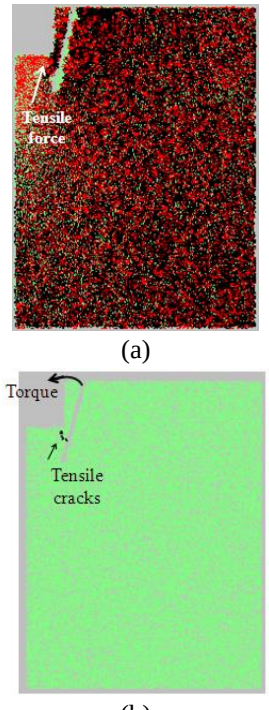

Fig. 6 (a) The parallel bond force distribution in the models at a state before crack initiation occurs and (b) progress of tensile fractures in the models

Table 3 Mechanical properties of joint set (Amuzesh *et al.* 2004)

c (MPa)	ϕ(°)	Normal stiffness (GPa/m)	Shear stiffness (GPa/m)
0.05	25.17	3.7	0.37

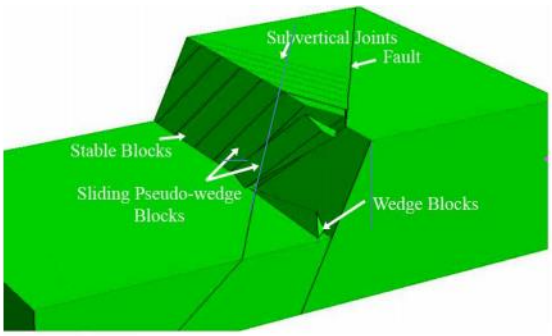

Fig. 7 Block model of Sarcheshmeh pseudo-wedge failure

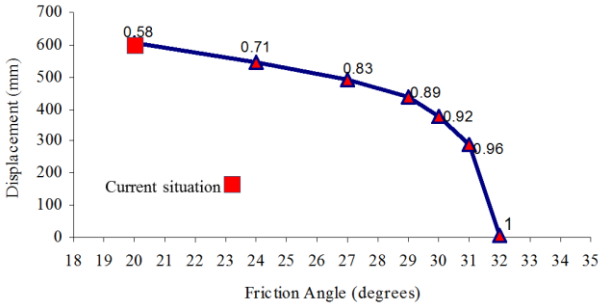

Fig. 8 Maximum displacement versus friction angle along with corresponding safety factor

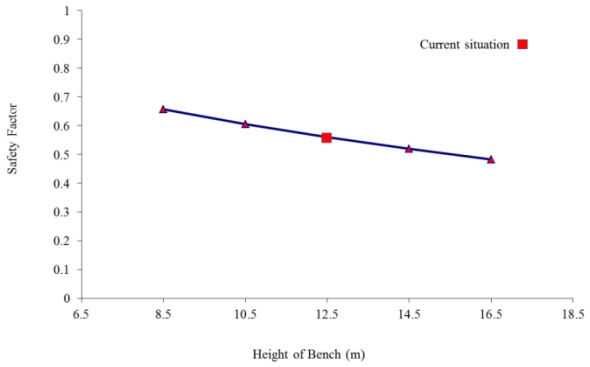

Fig. 9 Variation of *FS* with bench height

4. Block analysis

A block analysis of the Sarcheshmeh pseudo-wedge failure was carried out considering a hypothetical fracture from the bench toe to the fault plane. The strength properties of the fracture representing the rock bridge failure were considered the same as those of the pre-existing joint set. Three-dimensional distinct element code (3DEC), which is capable of modeling large displacements and rotations of discrete blocks (Cundall 1988, Hart *et al.* 1988, Itasca Consulting Group Inc. 1999a), was employed.

Considering low-stress conditions in the mine wall, deformation of intact rock is negligible compared to the displacements along the discontinuities and therefore, a rigid block model satisfied the block analysis. The only parameter of rock blocks required here was its density having a value of 2700 kg/m^3.

The Coulomb slip model was assigned as the constitutive model of joints. Table 3 presents the mechanical properties of the joint set used in the 3DEC model. The joint set has a mean spacing of 2 m (Panahi *et al.* 2001).

When the thickness of filling materials (t) exceeds the amplitude of discontinuity asperities (a), the joint shear strength is mainly controlled by the filling material (Fereidooni 2017, Indraratna *et al.* 2014, Khosravi *et al.* 2016). If the ratio of t/a reaches 3, the joint shear strength is reduced to the strength of the filling material (Goodman *et al.* 1972). Therefore, the strength properties of the clayey filling, mentioned earlier, were considered for the fault.

Fig. 7 shows the numerical simulation of the Sarcheshmeh psudo-wedge instability. As can be seen, there are two types of blocks sliding: wedge blocks, which are kinematically active; and pseudo-wedge blocks, which are first kinematically passive and are activated by the rock bridge failure at the bench toe.

4.1 Back analysis and model calibration

For the block analysis in which the purpose is to study the displacements, it is necessary to know values of normal and shear stiffnesses of the fault as the main slip surface. The shear stiffness (k_s) is quite important, whereas the normal stiffness (k_n) has a small role in modeling of shear displacements. Considering the high thickness of the clayey filling, it is expected that the fault behaves plastically and has very low stiffness values. However, there were no measurements of the fault stiffnesses. Hence, a back analysis was carried out to estimate the fault stiffness values based on field observation of displacements. As shown in Fig. 1, the wedge blocks first slide on the fault plane utterly, and then the pseudo-wedge blocks commence sliding. With increasing the size of the pseudo-wedge blocks, their displacements are gradually stabilized due to the increase of the rock bridge at the toe.

The values of normal and shear stiffnesses of the fault in the 3DEC model were varied assuming a constant ratio of 10 (k_n/k_s=10) such that the same behavior was observed in the model (Fig. 7). The normal and shear stiffnesses were consequently back-calculated 30 kPa/m and 3 kPa/m, respectively, and the model was calibrated.

4.2 Calculation of safety factor

A factor of safety (*FS*) is required to quantify the pseudo-wedge instability and to study the influence of different parameters. Dawson *et al.* (1999) proposed the method of shear strength reduction to calculate the safety factor in numerical analyses such as DEM (Dawson *et al.* 1999). To determine *FS* of the pseudo-wedge failure, 3DEC models were run for a series of trial factors of safety (FS_{trial}) in which the value of the fault friction angle was adjusted according to the equation below (Dawson *et al.* 1999)

$$\emptyset_{trial} = \arctan\left(\frac{1}{FS_{trial}}\tan\emptyset\right) \quad (1)$$

where ϕ and ϕ_{trial} are the actual and trial friction angles of the fault, respectively. The value of FS_{trial} was then varied using the bracketing technique until the slope was on the

verge of failure. In this case, the value of FS_{trial}=0.58 was considered to be the safety factor of the pseudo-wedge failure. The small value of safety factor suggests a progressive failure as happened at the pseudo-wedge failure in reality.

Fig. 8 shows the maximum displacement versus the friction angle along with the corresponding safety factor. As can be seen, the trial friction angle of ϕ_{trial}=32˚ corresponds to the safety factor of 1. The factor of safety typically used for rock slopes is in the range of 1.2-1.4 (Wyllie and Mah 2004).

5. Remedial measures based on geometry modification

The practical solution to prevent the Sarcheshmeh pseudo-wedge failure is to modify geometry of the failure area (Karimi Nasab, 2001). This section investigates the influence of geometrical characteristics of the mine wall on its stability using the block analysis.

5.1 Influence of bench height

The variation of *FS* for the different values of the bench height is plotted in Fig. 9. As can be seen, the more the height of the bench, the less the factor of safety is. However, the influence of this parameter on the stability is not noticeable so that the safety factor still remains below 1 when the height of bench is reduced to 8.5 m.

5.2 Influence of orientation

Fig. 10 shows the impact of the wall orientation on the factor of safety. As can be seen, *FS* drastically increases as the dip direction of the wall decreases, so that the factor of safety reaches above 1 with a 10-degree decrease of the dip direction. In fact, with increasing the wall dip direction, a smaller number of kinematically active wedges are formed.

5.3 Influence of slope angle

As can be seen in Fig. 11, the higher the slope of the wall, the lower the factor of safety is. The safety factor shows high sensitivity to the slope angle so that a 10-degree decrease in the bench dip results in a safety factor of 1.35. In addition, the possibility of the wedge block formation decreases with decreasing the bench slope.

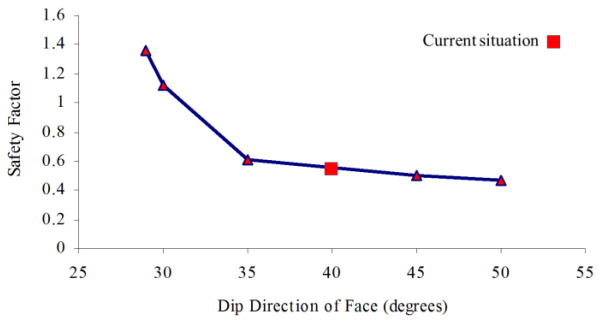

Fig. 10 Variation of *FS* with dip direction of wall

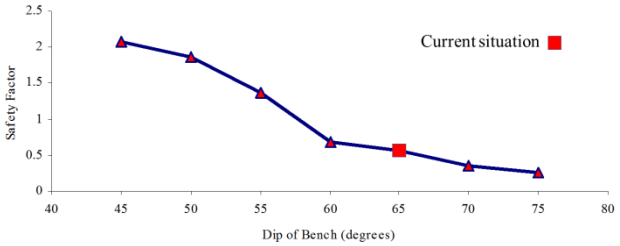

Fig. 11 Variation of *FS* with bench dip

6. Conclusions

From the kinematic point of view, most parts of the Sarcheshmeh pseudo-wedge failure are infeasible; however, they have become unstable over time. In order to investigate behavior of the rock bridge at the toe, a cross section of the infeasible areas of the failure was modeled PFC2D. The calibrated PFC model indicated development of tensile cracks between the slope toe and the fault due to the gravitational effect of the rock slope and the torque around the rock bridges.

A block analysis of the instability was carried out considering a hypothetical fracture representing the rock bridge failure. There are two types of blocks sliding: wedge blocks, which are kinematically active; and pseudo-wedge blocks, which are first kinematically passive and are activated by the rock bridge failure at the bench toe. A factor of safety of 0.58 was calculated using a DEM analysis in conjunction with the technique of shear strength reduction. Modification of geometry of the failure area was investigated as a practical solution to prevent the pseudo-wedge failure. The results showed that the influence of the bench height on the stability is not noticeable. On the other hand, the factor of safety drastically increases as the dip and dip direction of the wall decrease, so that its value reaches above 1 with a 10-degree decrease of them. Since a slope angle decrease results in higher stripping ratios and exploitation costs, it is suggested that the modification of the wall orientation is followed in the areas susceptible of the pseudo-wedge instability.

Acknowledgements

The authors would like to thank Dr. Saeed Karimi Nasab for providing geomechanical data. We also extend our gratitude to Dr. Mostafa Asadizadeh for his kind help.

References

Agliardi, F., Crosta, G.B., Meloni, F., Valle, C. and Rivolta, C. (2013), "Structurally-controlled instability, damage and slope failure in a porphyry rock mass", *Tectonophys.*, **605**, 34-47.

Amuzesh, M., Karimi Nasab, S., Atashpanjeh, A. and Babaie, B. (2004), "Stability analysis of the Sarcheshmeh pseudowedge failure based on the Hoek and Brown criteria", *Proceedings of the 2nd Iranian Rock Mechanics Conference*, Tehran, Iran, December.

Babanouri, N. and Dehghani, H. (2017), "Investigating a potential reservoir landslide and suggesting its treatment using limit-

equilibrium and numerical methods", *J. Mountain Sci*., **14**(3), 432-441.
Babanouri, N., Mansouri, H., Nasab, S.K. and Bahaadini, M. (2013), "A coupled method to study blast wave propagation in fractured rock masses and estimate unknown properties", *Comput. Geotech*., **49**, 134-142.
Blake, W. (1968), "Finite element model study of slope modification at the Kimbley pit", *Soc. Min. Eng. AIME*, **241**, 525-532.
Bonilla-Sierra, V., Scholtès, L., Donzé, F. and Elmouttie, M. (2015), "DEM analysis of rock bridges and the contribution to rock slope stability in the case of translational sliding failures", *J. Rock Mech. Min. Sci*., **80**, 67-78.
Corkum, A.G. and Martin, C.D. (2004), "Analysis of a rock slide stabilized with a toe-berm: A case study in British Columbia, Canada", *J. Rock Mech. Min. Sci*., **41**(7), 1109-1121.
Cundall, P.A. (1988), "Formulation of a three-dimensional distinct element model-Part I. A scheme to detect and represent contacts in a system composed of many polyhedral blocks", *J. Rock Mech. Min. Sci. Geomech. Abstr*., **25**(3), 107-116.
Cundall, P.A. and Strack, O.D.L. (1979), "A discrete numerical model for granular assemblies", *Geotechnique*, **29**(1), 47-65.
Cundall, P.A. and Strack, O.D.L. (1999), *Particle Flow Code in 2 Dimensions*, Itasca Consulting Group Inc.
Dawson, E.M., Roth, W.H. and Drescher, A. (1999), "Slope stability analysis by strength reduction", *Geotechnique*, **49**(6), 835-840.
Eberhardt, E., Stead, D. and Coggan, J.S. (2004), "Numerical analysis of initiation and progressive failure in natural rock slopes-the 1991 Randa rockslide", *J. Rock Mech. Min. Sci*., **41**(1), 69-87.
Faramarzi, L., Zare, M., Azhari, A. and Tabaei, M. (2016), "Assessment of rock slope stability at Cham-Shir Dam Power Plant pit using the limit equilibrium method and numerical modeling", *Bull. Eng. Geol. Environ*., **76**(2), 783-794.
Fereidooni, D. (2017), "Influence of discontinuities and clay minerals in their filling materials on the instability of rock slopes", *Geomech. Geoeng*., **13**(1), 11-21.
Gao, Y., Wu, D., Zhang, F., Lei, G.H., Qin, H. and Qiu, Y. (2016), "Limit analysis of 3D rock slope stability with non-linear failure criterion", *Geomech. Eng*., **10**(1), 59-76.
García López-Davalillo, J.C., Monod, B., Alvarez-Fernandez, M.I., Herrera Garcia, G., Darrozes, J., Gonzalez-Nicieza, C. and Olivier, M. (2014), "Morphology and causes of landslides in Portalet area (Spanish Pyrenees): Probabilistic analysis by means of numerical modelling", *Eng. Fail. Anal*., **36**, 390-406.
Ghazvinian, A., Sarfarazi, V., Schubert, W. and Blumel, M. (2012), "A study of the failure mechanism of planar non-persistent open joints using PFC2D", *Rock Mech. Rock Eng*., **45**(5), 677-693.
Goodman, R.E., Heuze, F.E. and Ohnishi, Y. (1972), "Research on strength, deformability, water pressure relationship for fault in direct shear", University of California, Berkeley, Berkeley, California, U.S.A.
Hart, R., Cundall, P.A. and Lemos, J. (1988), "Formulation of a three-dimensional distinct element model-Part II. Mechanical calculations for motion and interaction of a system composed of many polyhedral blocks", *J. Rock Mech. Min. Sci. Geomech. Abstr*., **25**, 117-125.
Huang, D., Cen, D., Ma, G. and Huang, R. (2015), "Step-path failure of rock slopes with intermittent joints", *Landslides*, **12**(5), 911-926.
Indraratna, B., Premadasa, W., Brown, E.T., Gens, A. and Heitor, A. (2014), "Shear strength of rock joints influenced by compacted infill", *J. Rock Mech. Min. Sci*., **70**, 296-307.
ISRM. (1978), "Suggested methods for determining tensile strength of rock materials", *J. Rock Mech. Min. Sci. Geomech. Abstr*., **15**(3), 99-103.
Itasca Consulting Group Inc. (1999a), *3DEC User's Guide*, Minneapolis, Minnesota, U.S.A.
Itasca Consulting Group Inc. (1999b), *Particle Flow Code in 2 Dimensions (PFC2D) Version 3.10 User's Manual*, Minneapolis, Minnesota, U.S.A.
Jiang, Q., Qi, Z., Wei, W. and Zhou, C. (2015), "Stability assessment of a high rock slope by strength reduction finite element method", *Bull. Eng. Geol. Environ*., **74**(4), 1153-1162.
Kanungo, D.P., Pain, A. and Sharma, S. (2013), "Finite element modeling approach to assess the stability of debris and rock slopes: A case study from the Indian Himalayas", *Nat. Hazards*, **69**(1), 1-24.
Karimi Nasab, S. (2001), "Remedial measures for Sarcheshmeh pseudowedge failure", *Proceedings of the 1st Iranian Rock Mechanics Conference*, Tehran, Iran, January.
Khosravi, A., Serej, A.D., Mousavi, S.M. and Haeri, S.M. (2016), "Effect of hydraulic hysteresis and degree of saturation of infill materials on the behavior of an infilled rock fracture", *J. Rock Mech. Min. Sci*., **88**, 105-114.
Latha, G.M. and Garaga, A. (2010), "Stability analysis of a rock slope in Himalayas", *Geomech. Eng*., **2**(2), 125-140.
Lombardi, M., Cardarilli, M. and Raspa, G. (2017), "Spatial variability analysis of soil strength to slope stability assessment", *Geomech. Eng*., **12**(3), 483-503.
Pain, A., Kanungo, D.P. and Sarkar, S. (2014), "Rock slope stability assessment using finite element based modelling-examples from the Indian Himalayas", *Geomech. Eng*., **9**(3), 215-230.
Panahi, M., Afsarinejad, M., Jalalifar, H. and Karimi Nasab, S. (2001), "Discontinuity information processing in slope stability in Sarcheshmeh copper mine", *Proceedings of the 1st Conference of Iran Open Pit Mines*, Kerman, Iran, October.
Potyondy, D.O. and Cundall, P.A. (2004), "A bonded-particle model for rock", *J. Rock Mech. Min. Sci*., **41**(8), 1329-1364.
Sarfarazi, V., Ghazvinian, A., Schubert, W., Blumel, M. and Nejati, H.R. (2014), "Numerical simulation of the process of fracture of echelon rock joints", *Rock Mech. Rock Eng*., **47**(4), 1355-1371.
Scholtès, L. and Donzé, F.V. (2015), "A DEM analysis of step-path failure in jointed rock slopes", *Comptes Rendus Mécanique*, **343**(2), 155-165.
Shahabpour, J. (1982), "Aspects of alteration and mineralization at the Sar-Cheshmeh copper-molybdenum deposit", Ph.D. Dissertation, University of Leeds, Leeds, West Yorkshire, U.K.
Shamekhi, E. and Tannant, D.D. (2015), "Probabilistic assessment of rock slope stability using response surfaces determined from finite element models of geometric realizations", *Comput. Geotech*., **69**, 70-81.
Shi, C., Li, D., Chen, K. and Zhou, J. (2016), "Failure mechanism and stability analysis of the Zhenggang landslide in Yunnan Province of China using 3D particle flow code simulation", *J. Mountain Sci*., **13**(5), 891-905.
Sjöberg, J. (1999), "Analysis of large scale rock slopes", Ph.D. Dissertation, Luleå University of Technology, Luleå, Sweden.
Stacey, T.R. (1970), "The stresses surrounding open-pit mine slopes", *Plan. Open Pit Mines*, 199-207.
Stead, D., Eberhardt, E. and Coggan, J.S. (2006), "Developments in the characterization of complex rock slope deformation and failure using numerical modelling techniques", *Eng. Geol*., **83**(1), 217-235.
Tiwari, G. and Latha, G.M. (2016), "Design of rock slope reinforcement: An Himalayan case study", *Rock Mech. Rock Eng*., **49**(6), 2075-2097.
Wang, S., Huang, R., Ni, P. and Jeon, S. (2017), "Advanced discretization of rock slope using block theory within the framework of discontinuous deformation analysis", *Geomech. Eng*., **12**(4), 723-738.
Waterman, G.C. and Hamilton, R.L. (1975), "The Sar Cheshmeh

porphyry copper deposit", *Econ*. *Geol*., **70**(3), 568-576.
Wyllie, D.C. and Mah, C. (2004). *Rock Slope Engineering: Civil and Mining*, CRC Press.
Yoon, J. (2007), "Application of experimental design and optimization to PFC model calibration in uniaxial compression simulation", *J*. *Rock Mech*. *Min*. *Sci*., **44**(6), 871-889.
Zheng, H., Liu, F.D. and Li, G.C. (2007), "On the assessment of failure in slope stability analysis by the finite element method", *Rock Mech*. *Rock Eng*., **41**(4), 629-639.

CC